*Progress In Electromagnetics Research C, Vol. 127, 227–237, 2022*

# A Directional Wide-Band Antipodal Vivaldi Antenna for Imaging Applications

**Amit Birwal[1, *], Kamlesh Patel[1], and Sanjeev Singh[2]**

**Abstract**—This paper presents a new compact directional antipodal Vivaldi antenna that can be employed in modern imaging applications. To obtain wide-band impedance bandwidth in the proposed antenna, a staircase slot is introduced in both a tapered region and a triangular ground plane. In addition, by means of introducing a parasitic patch close to the centre of radiators, more directional radiation characteristic is attained within the operational bandwidth. Based on the simulation results, the antenna designed on an FR4 substrate provides a wide impedance bandwidth ($S_{11} < -10$ dB) of 6.2 GHz (3.8–10 GHz) with a gain between 3.5 and 7.5 dB, which is suitable for a variety of imaging applications. The designed single feed antenna is compact, low profile, and trimmed to provide a triangular geometry with light weight. To validate the directional radiation performance, the proposed antenna is fabricated and integrated with a signal generator and spectrum analyzer to obtain the image of a uniform target cylinder using the standard back-projection Radon transform algorithm. The proposed setup along with the algorithm is promising for the civil and medical applications on applying to other shapes of objects.

## 1. INTRODUCTION

There has always been a great demand for wideband antennas for military and commercial applications based on wireless communication. Microwave imaging is widely used in many areas, such as material science, object scanning, and remote sensing applications. This technique is used to generate images of the target object under test. The operating frequency can be of the order of a few GHz. It is in demand in both military and commercial applications. Microwave imaging techniques have been widely explored for imaging two-dimensional (2D) or three-dimensional (3D) targets in front of or through wall objects [1]. Imaging concrete structures to detect manufacturing flaws along with non-destructive testing is a challenging area [2]. The antenna required to cater to the demand for microwave imaging systems should have wide bandwidth, small size, low weight, and high directional gain within the operating bandwidth. To obtain the desired level of image resolution, an ultra-wideband (UWB) technology is adopted, which can help to get more penetration depth inside the target objects based on the wide frequency bands. Usually, UWB antennas with directional radiation patterns are preferred. Therefore, the Vivaldi antenna is the best suitable antenna for such applications as it provides around 6 dB of gain with limited impedance bandwidth due to the transition between microstrip and slot line at the feeding network [3]. The simplest geometry of the Vivaldi antenna reported by [4] is known as an antipodal Vivaldi antenna, where the two radiators are printed on either side of the antenna substrate. The antenna supports a wide bandwidth with a linearly polarized wave. In addition, such an antenna helps to achieve the requirement of mobility for any small system.

*Received 22 October 2022, Accepted 14 December 2022, Scheduled 18 December 2022*
* Corresponding author: Amit Birwal (amit.birwal@south.du.ac.in).
[1] Department of Electronic Science, University of Delhi South Campus, New Delhi-110022, India. [2] Institute of Informatics and Communication, University of Delhi South Campus, New Delhi-110022, India.

Many challenging issues must be taken care of when a Vivaldi antenna is designed. One such issue is maintaining a stable radiation pattern over a wide bandwidth. Usually, such antennas behave as resonant antennas at lower frequencies and become more directional or non-resonant at higher frequencies. In recent literature, many designs of Vivaldi antennas have been reported to improve the radiation performance at high frequencies. An elliptical parasitic patch is introduced in [5], which improves the gain at high frequencies without impacting the performance at a lower frequency. In [6], an elliptically tapered antipodal Vivaldi antenna is presented with comb-shaped slits available in both top and bottom radiators to improve the gain at lower frequencies and overall front-to-back ratio. The reported antenna is ultra-wideband from 1.6 to 18 GHz with a good penetration depth. It is suitable for imaging applications. A compact antipodal Vivaldi antenna is reported in [7] having a working bandwidth from 3.1 to 10.6 GHz and is fabricated on RO3006 and FR4 substrates with low cross-polarization and gain around 2–5 dB. Also, in [8], another compact antipodal Vivaldi antenna is described, where structural modifications in terms of an L-shaped slot are made in both radiating elements to increase the overall electrical length and make the antenna operational at a lower frequency band of 3.7–5.2 GHz. Many modifications in the flare size with different shapes have been reported, such as ellipse [8], circle [9], and Chebyshev [10]. These modifications increase the aperture area of the antenna and thus increase the overall gain. But out of these reported flare structures, the elliptical flare structure is most commonly used because of its simple design and easy tuning rate and offers a very wide impedance bandwidth up to 25 : 1. Some designs reported in the literature are using dielectric lens as a director after placing it in the middle of two flares. As reported in [11], these dielectric lenses with high permittivity increases act as a waveguide to direct the radiation towards the centre of the aperture, which helps in increasing the gain of the antenna. For this purpose, many dielectric shapes, including metamaterials, have been reported in the literature [12]. It is reported in [13] that an antipodal Vivaldi antenna with an array increases the overall gain of the antenna. However, such a structure has many drawbacks, including side lobes and mutual coupling between the elements. To reduce the distance between the elements, many researchers have tried other shapes to overcome these effects.

In this article, a compact directional antipodal Vivaldi antenna (AVA) intended to work from 3.8 to 10 GHz is presented and can be employed in modern imaging applications. Modification in terms of slotting the radiators is employed to improve the impedance bandwidth. A parasitic patch is incorporated in between the radiators to improve the directional characteristics of the antenna. Finally, by using a pair of the proposed AVAs along with a signal generator and spectrum analyzer, a potential imaging application can be considered by varying the scanning distance to reconstruct the image of a target object.

## 2. ANTENNA DESIGN AND EVOLUTION PROCESS

The geometry of the proposed antipodal Vivaldi antenna (AVA) is shown in Fig. 1. The planar antenna consists of a top radiator and a bottom radiator with a staircase slot in each radiator. A triangle-shaped ground is inserted at the bottom to enhance the impedance bandwidth, as shown in Fig. 1(a). The top microstrip line is excited through a 50 Ω feed line. The antenna is fabricated on both sides of the FR4 substrate material ($\epsilon_r = 4.4$, $h = 1.6$ mm and tan = 0.04) with dimensions of $45.5 \times 40 \times 1.6\,\text{mm}^3$ as shown in Fig. 1(b), showing both the top and bottom views of the antenna.

The antenna design, feeding, and simulation are carried out using commercially available CST Microwave Studio software. The final optimized parameters of the antenna are given in Table 1.

To get a better understanding of the proposed AVA, the main evolution steps consisting of slots and parasitic patch incorporation in conventional AVA are demonstrated in Fig. 2. The first antenna shown in Fig. 2(a) is a simple wide-band AVA as reported in [7] with some design modification in triangular ground plane and radiators. It is observed that with the $S_{11}$ characteristics shown in Fig. 3, the maximum return loss is limited up to −25 dB. To improve the return loss, a square staircase slot of side $S = 0.5$ mm is incorporated in each radiator as shown in Fig. 2(b). The introduced staircase slot improves the $S_{11}$ up to −45 dB and −30 dB at 5.4 and 7.1 GHz, respectively. To make the antenna more directional, a parasitic patch is introduced in the middle of the top and bottom radiators as shown in Fig. 2(c), which enhances the gain and radiation characteristics of the antenna as shown in Fig. 4 and Fig. 5. Thus, by adding the parasitic patch, a minor improvement in front-to-back ratio and

**Table 1.** Dimensions of the proposed antenna.

| Parameter | Value (mm) | Parameter | Value (mm) |
|---|---|---|---|
| $L$ | 45.5 | $W_g$ | 16 |
| $W$ | 40 | $W_f$ | 2.2 |
| $L_1$ | 9.14 | $S$ | 0.5 |
| $W_p$ | 4 | $L_2$ | 15 |
| $L_3$ | 6 | $H$ | 1.6 |

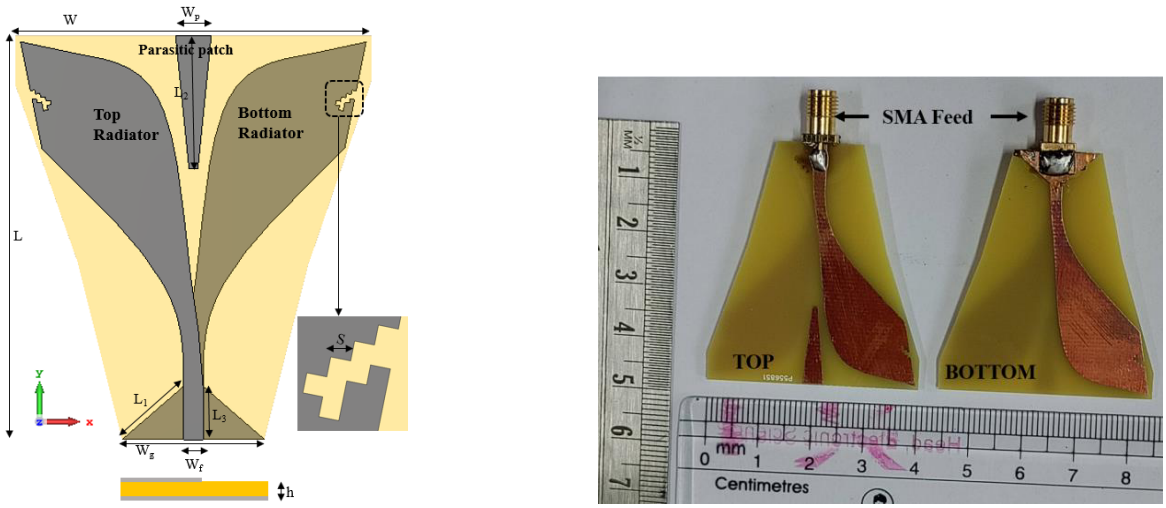


(a) (b)

**Figure 1.** Geometry of the (a) proposed antipodal Vivaldi antenna, (b) top and bottom view of fabricated prototype.

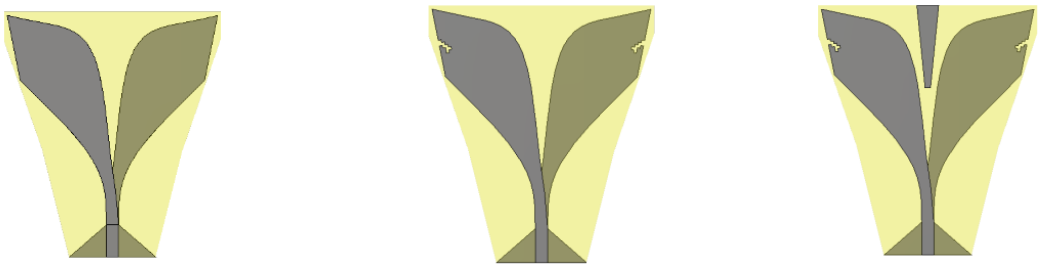

(a) (b) (c)

**Figure 2.** Evolution design of the proposed AVA antenna, (a) Simple AVA, (b) Slotted AVA, (c) Slotted & Parasitic patch AVA.

amplification in gain are found.

The radiating properties of the proposed AVA are optimized by varying the stub dimensions and arrangement of the parasitic patch. As stated in Section 1, the AVA acts as a resonant antenna at lower frequencies and a non-resonant or travelling wave antenna at higher frequencies. Usually, frequency operation depends on the maximum separation width ($W$) of the antenna, which is approximately half the wavelength within the lower frequency band. The radiation at a higher frequency is produced due to the flow of travelling wave current across the flare edges of both, top and bottom radiators. The

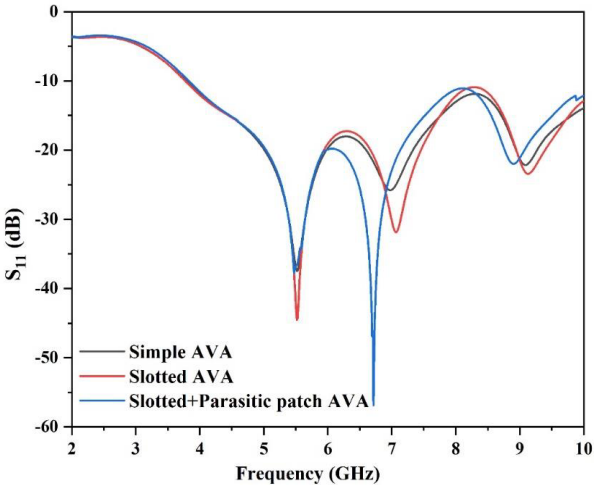


**Figure 3.** Simulated $S_{11}$ with different AVA designs during evolution stages.

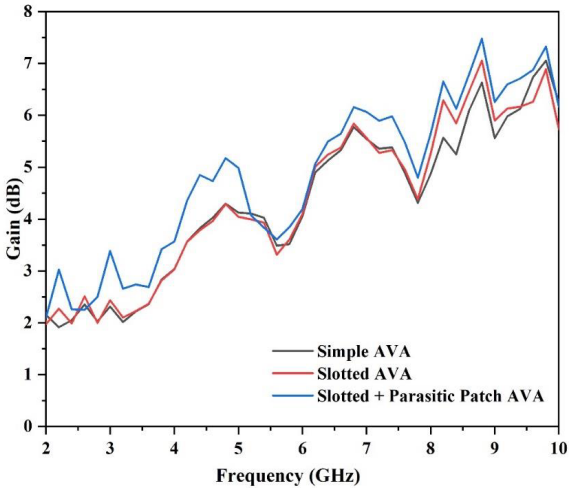


**Figure 4.** Simulated gain with different AVA designs during evolution stages.

radiated waves are detached from the antenna as the flare aperture increases and give rise to space waves. To keep these radiated fields in the end-fire direction, the phase difference of the wave travelling in both radiators should be 180° apart. The radiators are kept in an antipodal configuration.

With increasing the operating frequency in the proposed AVA, unwanted radiation occurs due to this travelling wave current across the flare section. As a result, the radiation performance degrades, and the antenna radiation and gain are reduced. With the introduction of a staircase slot in both radiators, improvement can be seen in the impedance bandwidth and radiation characteristics within the entire operating band. The AVA performance also depends upon the substrate height ($h$). As the substrate height increases, many undesired modes get excited, causing phase alteration of the travelling wave currents. To overcome such issues, a substrate height of 1.6 mm is selected, which is less than $0.03\lambda_o$, as reported [5], where $\lambda_o$ is the wavelength in free space. The long flare electrical length of AVA is responsible for its wideband operation but also limits the performance at a higher frequency due to the phase reversal issue reported in [5] across the flare length. The effective method to overcome this issue is the reduction of the flare rate, which in turn also decreases the flare opening.

So to address this performance issue at a higher frequency, a polygon-shaped parasitic patch is introduced in between the radiators without impacting the low-frequency response, as shown in Fig. 2(c). To better understand the effect of the parasitic patch, the electric field magnitudes with and without the parasitic patch are plotted in the $XY$-plane using the feature available at CST Microwave Studio as seen in Figs. 5(a) and (b). As shown in Fig. 6, there is a strong coupling of the field to the parasitic patch in Fig. 6(b), which aids in directing the radiation more toward the end-fire direction than the AVA without the parasitic patch in Fig. 6(a), where no parasitic patch is present. Thus, the coupling between the fields improves with the introduction of this parasitic patch, and the AVA overcomes the phase reversal issue and provides strong end-fire radiation. Although the electric field distribution shown here is for 7 GHz, similar results are also obtained for other frequencies within the operating band.

## 3. MEASUREMENT RESULTS AND DISCUSSION

A pair of Vivaldi antennas are fabricated on an FR4 board with the help of the photolithography technique, and measurements are carried out using the vector network analyzer R&S ZVH after connecting the SMA edge-mount connector. The reflection coefficient simulation result exported from the CST software is compared against the measurement results as shown in Fig. 7. It is observed that the measured impedance bandwidth of the antipodal Vivaldi antenna is around 6.2 GHz from 3.8 to 10 GHz, which is 90% with a central frequency of 6.9 GHz. As can be seen from Fig. 7, the addition of a parasitic patch does not significantly impact the return loss. However, the parasitic patch slightly

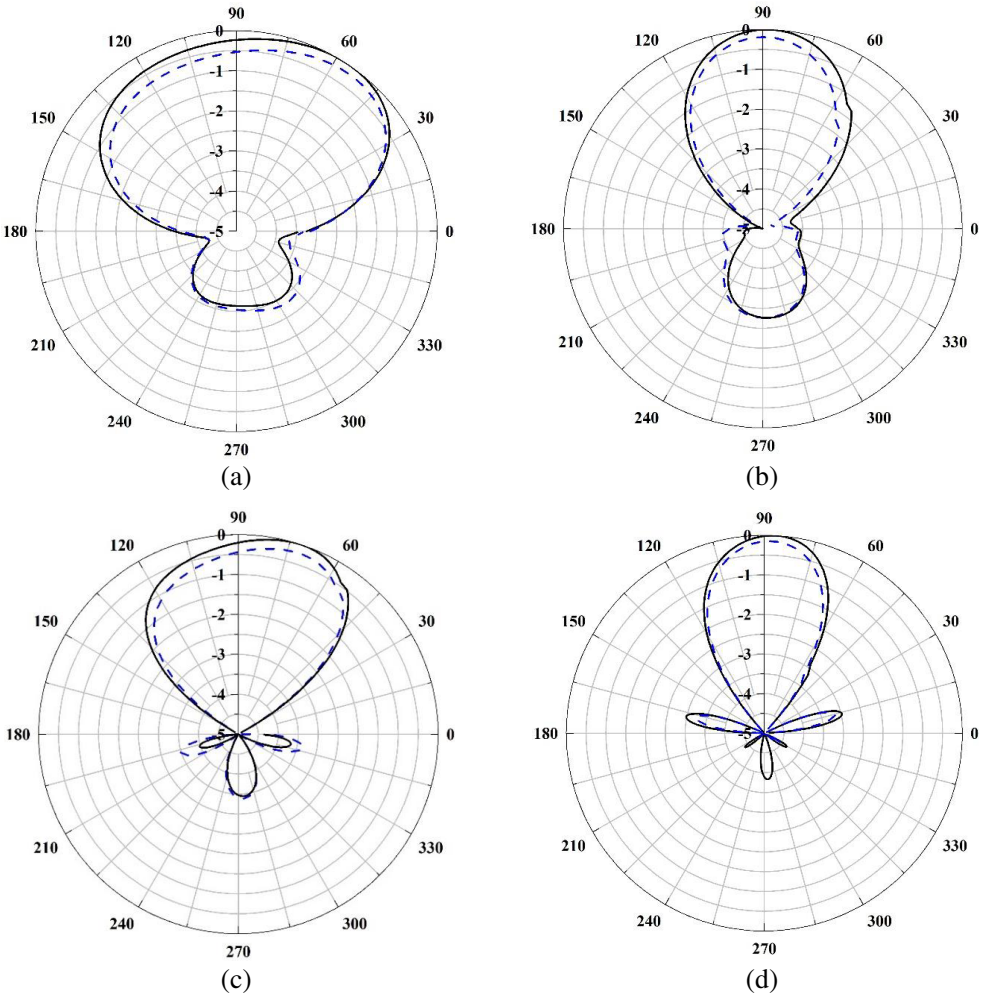


**Figure 5.** The simulated $E$-plane radiation patterns with (solid line) and without (dashed line) parasitic patch at (a) 5 GHz, (b) 6 GHz, (c) 7 GHz, (d) 9 GHz.

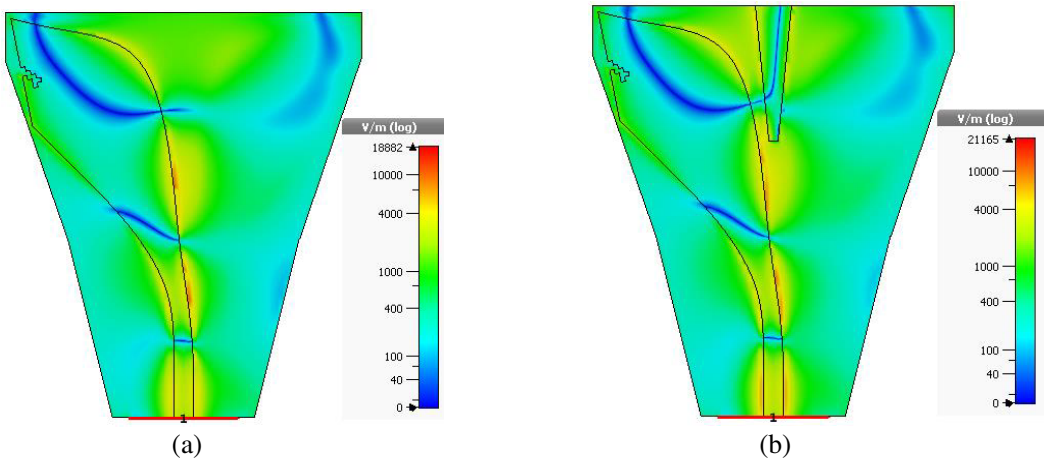


**Figure 6.** Electric field distribution of the proposed AVA (a) without and (b) with the parasitic patch at 7 GHz.

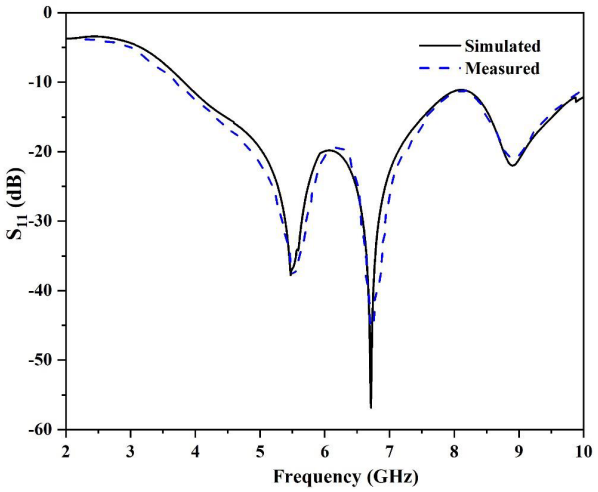


**Figure 7.** Simulated and measured $S_{11}$ of the proposed antenna.

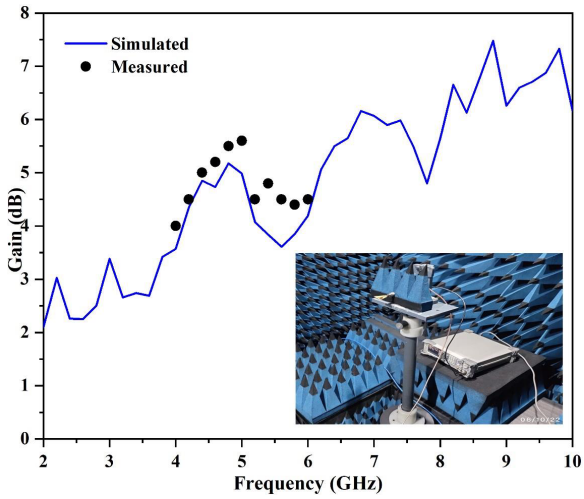


**Figure 8.** Simulated and measured the gain of the proposed AVA antenna.

improves the antenna gain, as seen in Fig. 8. A minor deviation is observed between the measurement and simulation due to misalignment errors that exist between the reference antenna and the antenna under test. Compared to the antenna without the parasitic patch, the antenna gain improves slightly at the lower frequency band around 5–6 GHz and is significantly better above this. Because of this directional property, the proposed antenna is a suitable candidate for microwave imaging applications, which will be discussed in the next section.

Table 2 compares the basic characteristics of the proposed antipodal Vivaldi antenna with previously reported antenna designs on different substrates. The antennas reported in the literature differ from each other in geometry, topology, and application type. The proposed antenna offers a simple geometry and compact size with moderate gain suitable for microwave imaging applications.

**Table 2.** A Comparison of the proposed antipodal Vivaldi antenna with other reported antennas.

| Ref. | Size ($mm^2$) | Frequency (GHz) | Minimum Return Loss (dB) | Gain (dB) | Application/Band |
|---|---|---|---|---|---|
| [1] | $74 \times 44$ | 8–16 | −37 | 7.8–10.8 | UWB |
| [5] | $140 \times 66$ | 7–32 | −27 | 0–12 | UWB, 5G |
| [6] | $120 \times 202$ | 1.6–18 | −46 | 7–15 | Concrete Beam imaging |
| [10] | $100 \times 100$ | 1–35 | −52 | 4.5–6.8 | UWB, 5G |
| [11] | $78 \times 44$ | 2.2–12 | −40 | Not given | Brest Cancer Detection |
| Prop. | $45.5 \times 40$ | 3.1–10 | −56 | 2–6 | UWB, Imaging |

## 4. MICROWAVE IMAGING APPLICATION OF THE PROPOSED VIVALDI ANTENNA

In this section, the proposed Vivaldi antenna for microwave imaging is discussed with the various steps involved in excitation, scanning and reconstruction mechanisms to obtain the impression of the target object. The image reconstruction algorithm is based on the Radon transform and parallel projections of the target object (TO) [14]. Here, the TO is exposed to a high-frequency wave, i.e., 5 GHz, while moving

the receiving antenna at various distances so that it minimizes the effect of diffraction and coupling caused by low-frequency waves. Since the high-frequency wave is more directional, it concentrates more on the TO placed between the transmitting and receiving antennas. Here, a 2-D image function $I(x, y)$ required to be reconstructed is first projected to a 1-D profile $g(\rho, \theta)$, where $\rho$ and $\theta$ are the distance and angle from the $Y$ and $X$ axes, as shown in Fig. 9. The 2-D image $I(x, y)$ is assumed to be a cross-sectional cut of the 3-D target object. The Radon transform maps the $I(x, y)$ to $g(\rho, \theta)$ for each arbitrary line, where each $g(\rho, \theta)$ value corresponds to the line integral of $I(x, y)$. The general expression of the function $g(\rho, \theta)$ can be written as

$$g(\rho, \theta) = \text{Radon Transform of } I(x, y) = \iint_{-\infty}^{\infty} I(x, y)\delta(x\cos\theta + y\sin\theta - \rho)dxdy \tag{1}$$

where $\delta$ is the impulse function. As shown in Fig. 9(a), the function $g(\rho_j, \theta_k)$ can be obtained by making a series of parallel projections $\rho_j$ along the scanning direction at an angle $\theta_k$ in terms of an electromagnetic wave generated by a transmitting antenna and received by a receiving antenna. Here each point, for example, $g(\rho_2, \theta_k)$ corresponds to the projected 2-D image $I(x, y)$ at $g(\rho = \rho_2,\ \theta = \theta_k)$. In MATLAB®, this transformation can be done by using a standard function called *radon*.

Now image reconstruction can be done by taking the Fourier transform of each $g(\rho, \theta)$ by transforming this time-domain $\rho$ to frequency domain $\omega$, i.e., $g(\rho, \theta)$ to $G(\omega, \theta)$, multiplying each Fourier transform $G(\omega, \theta_k)$ by the filter function $|\omega|$, and then the inverse Fourier transform and the integration of all $\theta_k$ to get the image of the target object $I(x, y)$, and this concept was adopted by many researchers and is commonly known as the Fourier-slice theorem [15] for image reconstruction.

$$I(x, y) = \int_{-\infty}^{\infty} |\omega| G(\omega, \theta) e^{j2\pi\omega\rho} d\omega \tag{2}$$

where $G(\omega, \theta)$ is the Fourier transform of $g(\rho, \theta)$ concerning $\rho$, i.e., $G(\omega, \theta) = \int_{-\infty}^{\infty} g(\rho, \theta) e^{-j2\pi\omega\rho} d\rho$. In MATLAB® this inverse transformation can be done by using a standard function called *iradon*.

To validate the technique presented in this paper, an experimental setup consisting of two symmetrical proposed Vivaldi antennas that act as transmitting and receiving antennas is designed, as shown in Fig. 10 based on Fig. 9(b). A cylindrical target object made up of hollow cardboard is placed in the scanning area. For this study, a cylindrical object is selected due to its symmetric nature across all the scan angles $\theta_k$, where only one measurement reading is required at any scan angle (let's say

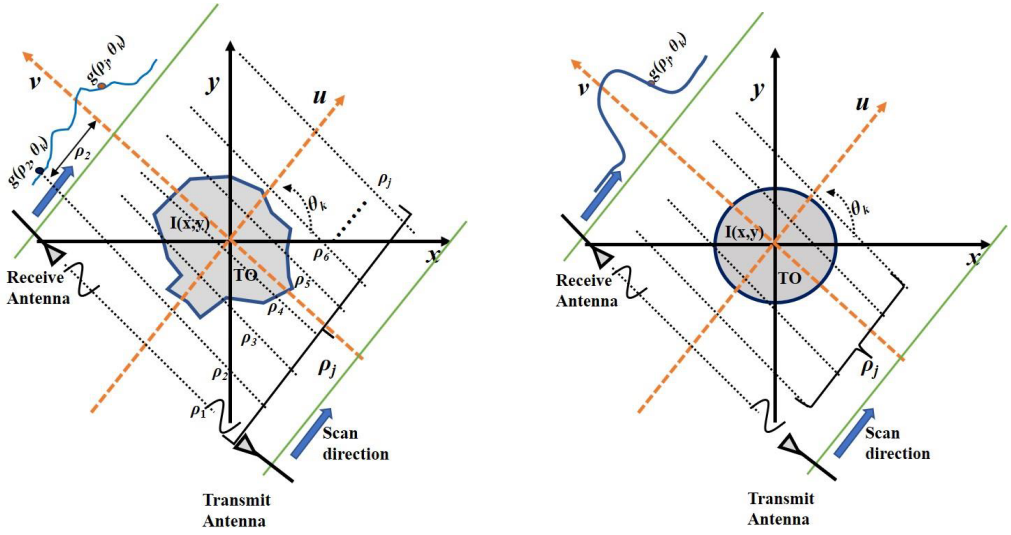


**Figure 9.** 1-D projection of a 2-D image, $I(x, y)$ is projected to $g(\rho_j, \theta_k)$, (a) an arbitrary image, (b) an image of a hollow cylindrical object.

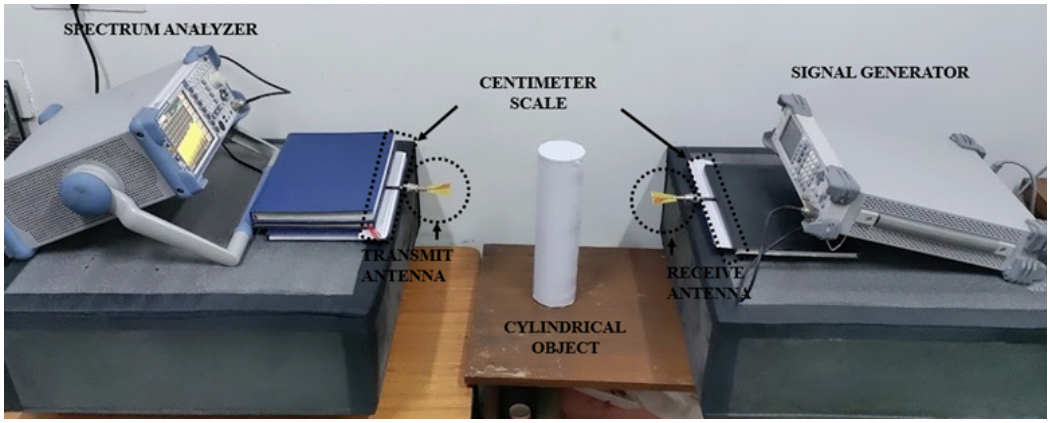


**Figure 10.** Scanning measurement setup with the uniform cylindrical object.

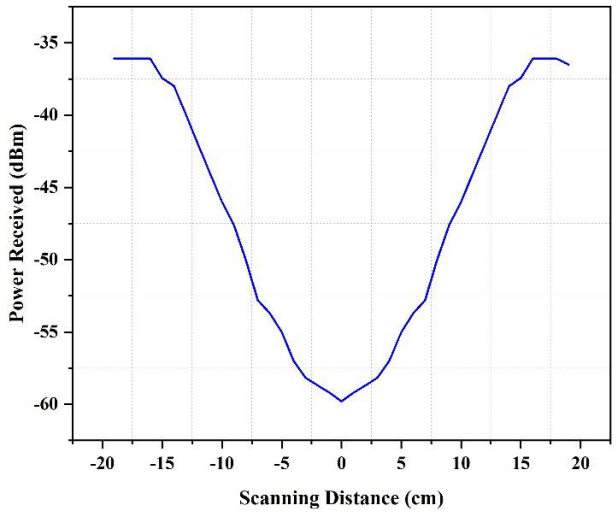


**Figure 11.** Received power profile (in dBm) of receiving Vivaldi antenna for various scanning distances.

$k = 1$) $\theta_1$ which will be the same for another measurement at different scan angles $\theta_k$ ($k = 2, 3, 4, \ldots$). An air-filled hollow cylinder of diameter 8.75 cm, height 30 cm with a cardboard thickness of 5 mm is placed in the middle of the scanning area. As shown in Fig. 10, the transmitting antenna (proposed Vivaldi antenna) is connected to the signal generator RIGOL® DSG3060, and the receiving antenna is connected to spectrum analyzer R&S® FSL6 for the received power.

For this study, a transmitting power of 0 dBm is selected at 5 GHz, and a corresponding received power is measured by scanning the receiving antenna from $-u$ to $+u$ direction at a step distance of 1 cm at any arbitrary scan angle $\theta$. For this study, the measurement is taken at a scanning distance of 1 cm. As can be seen in Fig. 11, the received power in free space is constant, i.e., $-36.1$ dBm beyond $\pm 16$ cm, where no target object exists between the transmitting and receiving antennas. Then, the received power starts to fall as the target object comes in the paths of the antenna pairs for the lesser scanning distance.

Further, when the receiving antenna reaches the middle of the target object at 0 cm, the received power drops to a minimum, i.e., from $-55$ to $-60$ dBm due to its circular shape. The power profile intensity depicted in Fig. 11 is a 1-D projected profile $g(\rho, \theta)$, equivalent to the Radon transform of the 2-D image $I(x, y)$ of cylindrical object, which is not transparent to the microwave signals. Thus, the use of proposed antennas pair at a high frequency not only reduces the diffraction problem but also generates the power profile intensity useful for imaging based on Radon transform.

The data from Fig. 11 is imported into MATLAB® and padded three times to increase the resolution of the reconstructed image before being used as the $g(\rho, \theta)$ function. Now, using the MATLAB *iradon* & *imshow* command on this $g(\rho, \theta)$ function, its Fourier and inverse Fourier transforms are obtained. The reconstructed image, also known as laminogram, is shown in Fig. 12 for various scan angles $\theta$. The back-projected image is blurry because all projections intersect at the common centre point without any filtering, as shown in Fig. 13(a).

To enhance the image resolution, a filtering function, consisting of a ramp filter with a hamming

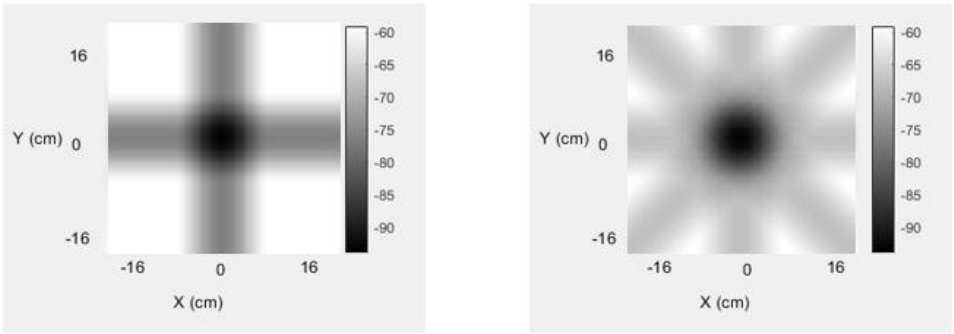


(a) (b)

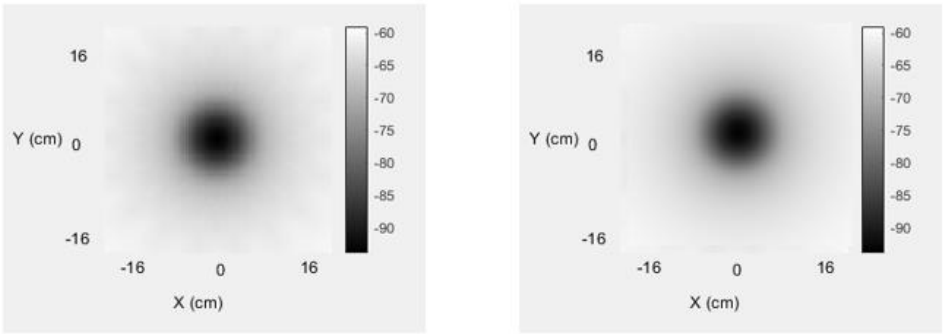


(c) (d)

**Figure 12.** Reconstructed image after back projections at various scan angles (a) 90°, (b) 45°, (c) 20° and (d) 1°.

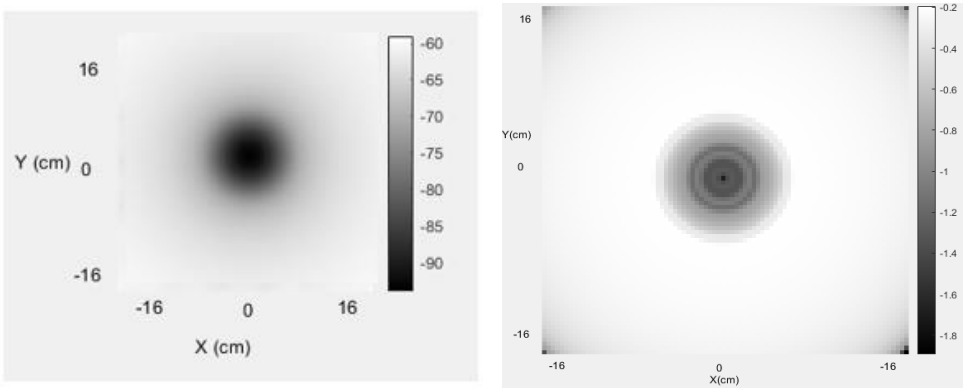


(a) (b)

**Figure 13.** Reconstructed image of a cylindrical object with 1° step of scan angle, (a) no filtering, (b) with filtering.

window, is applied to filter out the common intersection points. As expected for a cylinder, which is a symmetrical object, the back projection shows a similar profile for all the scan angles, and the final reconstructed image is shown in Fig. 13(b). Here, the image reconstruction procedure is applied to the cylindrical object. However, the same method can also be useful for other object types. Thus, the method described in this work is computationally simple and reconstructs the image using only the transmitted wave amplitude data, i.e., the received power profile coming from the non-transparent target object at various scan angles.

## 5. CONCLUSION

In this work, a new compact directional antipodal Vivaldi antenna is presented for modern imaging applications, which offers wide band and high gain due to the staircase slot and parasitic patch. This antenna consists of top and bottom radiating arms printed on both sides of a 1.6 mm-thick FR4 substrate, along with the parasitic patch in between. This makes the antenna an efficient directional radiator from the upper and bottom parts. The measured results are found in good agreement with the simulation, with an impedance bandwidth ($S_{11} < -10$ dB) of 6.2 GHz from (3.8–10 GHz). The microwave imaging method described in this work is computationally simple and reconstructs the image using only the transmitted wave amplitude data and the received power profile coming through the target object at various scan angles. It is shown that by using antipodal Vivaldi antennas and the Radon transform with filter back projection method, high-resolution imaging can be done, particularly for civil and medical applications.

## ACKNOWLEDGMENT

The present work is performed under the Faculty Research Programme FRP of the Institute of Eminence (IoE) scheme of the University of Delhi (Grant Ref Number: IoE/2021/12/FRP dated 31/08/2022). The authors also link to acknowledge the Indian Science Technology and Engineering Facilities Map (I-STEM) for providing access to the MATLAB platform.

## REFERENCES

1. Etesami, F., S. Khorshidi, S. Shahcheraghi, and A. Yahaghi, "Improvement of radiation characteristics of balanced antipodal Vivaldi antenna using transformation optics," *Progress In Electromagnetics Research M*, Vol. 56, 189–196, 2017.
2. Moosazadeh, M. and S. Kharkovsky, "Development of the antipodal Vivaldi antenna for detection of cracks inside concrete members," *Microwave and Optical Technology Letters*, Vol. 57, No. 7, 1573–1578, 2015.
3. Dixit, A. S. and S. Kumar, "A survey of performance enhancement techniques of antipodal Vivaldi antenna," *IEEE Access*, Vol. 8, 45774–45796, 2020.
4. Gazit, E., "Improved design of the Vivaldi antenna," *IEE Proceedings H (Microwaves, Antennas and Propagation)*, Vol. 135, No. 2, 89–92, IET Digital Library, 1988.
5. Nassar, I. T. and T. M. Weller, "A novel method for improving antipodal Vivaldi antenna performance," *IEEE Transactions on Antennas and Propagation*, Vol. 63, No. 7, 3321–3324, 2015.
6. Moosazadeh, M., S. Kharkovsky, J. T. Case, and B. Samali, "Antipodal Vivaldi antenna with improved radiation characteristics for civil engineering applications," *IET Microwaves, Antennas & Propagation*, Vol. 11, No. 6, 796–803, 2017.
7. Hood, A. Z., T. Karacolak, and E. Topsakal, "A small antipodal Vivaldi antenna for ultrawide-band applications," *IEEE Antennas and Wireless Propagation Letters*, Vol. 7, 656–660, 2008.
8. Lee, S., J. Hur, M. B. Heo, S. Kim, H. Choo, and G. Byun, "A suboptimal approach to antenna design problems with kernel regression," *IEEE Access*, Vol. 7, 17461–17468, 2019.
9. Bai, J., S. Shi, and D. W. Prather, "Modified compact antipodal Vivaldi antenna for 4–50-GHz UWB application," *IEEE Transactions on Microwave Theory and Techniques*, Vol. 59, No. 4, 1051–1057, 2011.

10. Gorai, A., A. Karmakar, M. Pal, and R. Ghatak, "A super wideband Chebyshev tapered antipodal Vivaldi antenna," *AEU-International Journal of Electronics and Communications*, Vol. 69, No. 9, 1328–1333, 2015.
11. Bourqui, J., M. Okoniewski, and E. C. Fear, "Balanced antipodal Vivaldi antenna with dielectric director for near-field microwave imaging," *IEEE Transactions on Antennas and Propagation*, Vol. 58, No. 7, 2318–2326, 2010.
12. Dixit, A. S. and S. Kumar, "A survey of performance enhancement techniques of antipodal Vivaldi antenna," *IEEE Access*, Vol. 8, 45774–45796, 2020.
13. Zhu, S., H. Liu, Z. Chen, and P. Wen, "A compact gain-enhanced Vivaldi antenna array with suppressed mutual coupling for 5G mmWave application," *IEEE Antennas and Wireless Propagation Letters*, Vol. 17, No. 5, 776–779, 2018.
14. Theofanopoulos, P. C., M. Sakr, and G. C. Trichopoulos, "Multistatic terahertz imaging using the radon transform," *IEEE Transactions on Antennas and Propagation*, Vol. 67, No. 4, 2700–2709, 2019.
15. Mirjahanmardi, S. H., "Microwave near-field imaging and material characterization," Ph.D. Thesis, UWSpace, 2020, http://hdl.handle.net/10012/15725.